ISEIS

Journal of Environmental Informatics 42(2) 108-122 (2023)

Journal of Environmental Informatics

www.iseis.org/jei

The Effects of Intra-Annual Variability of River Discharge on the Spatio-Temporal Dynamics of Saltmarsh Vegetation at River Mouth Bar: Insights from an Ecogeomorphological Model

S. Zheng[1, 2], W. Gao[1, 2, 3], D. Shao[1, 2, 4 *], W. Nardin[5], C. Gualtieri[6], and T. Sun[1, 2 *]

[1] State Key Laboratory of Water Environment Simulation, School of Environment, Beijing Normal University, Beijing 100875, China
[2] Yellow River Estuary Wetland Ecosystem Observation and Research Station, Ministry of Education, Dongying, Shandong 257200, China
[3] Research and Development Center for Watershed Environmental Eco-Engineering, Beijing Normal University, Zhuhai, Guangdong 519087, China
[4] Tang Scholar, Beijing Normal University, Beijing 100875, China
[5] Horn Point Laboratory, University of Maryland Center for Environmental Science, Cambridge, MD 21613, USA
[6] Department of Civil, Architectural and Environmental Engineering, University of Napoli Federico II, Via Claudio 21, Napoli 80125, Italy

Received 30 July 2021; revised 12 November 2021; accepted 06 March 2023; published online 10 August 2023

ABSTRACT. Natural or human-induced intra-annual variation of river discharge alters estuarine hydrological regimes and further affects habitat conditions for saltmarsh vegetation, particularly at the river mouth bar. In this study, numerical experiments were performed in Delft3D to simulate the evolution of a schematized river mouth bar under prototypical unsteady river discharge scenarios. The simulated hydrodynamic and morphodynamic changes were used to drive a vegetation dynamics model developed based on Spartina alterniflora in real time to model the resultant vegetation responses throughout the plant life history. Our results show that the imposed seasonal high flow can create more potential suitable habitat for the vegetation expansion and at the same time, cause marsh erosion through flood-induced drag force and substrate erosion. The overall effect of the trade-off between expansion and erosion depends on the timing, magnitude and duration of the high flow as well as its carried sediment concentration, leading to three vegetation response regimes, namely, minimal impact with small flood, erosion with big flood and low sediment supply, and expansion with big flood and high sediment supply. Besides, the timing of the high flow determines whether the vegetation has enough time to occupy the newly created subaerial area after the high flow and thereby affects the overall saltmarsh extent. The proposed vegetation response regimes are verified in principle in real cases such as Yellow River Estuary, Wax Lake Delta and Yangtze River Estuary. Our findings can help inform water diversion projects in river deltas to restore coastal wetlands in terms of suitable sediment supply and timing, etc.

Keywords: ecogeomorphological model, river mouth bar, river deltas, saltmarsh, intra-annual variation, unsteady river discharge

1. Introduction

Saltmarshes are one of the most important ecosystems located between land and ocean, which provide many important ecosystem functions such as carbon fixation and nutrient cycling (Barbier et al., 2008; de Groot et al., 2012). Estuarine saltmarshes are widely found in large river deltas, which are subject to terrestrial and marine forcing such as river discharge, tides and waves (Fagherazzi et al., 2012). Increasing human activeties in the catchment such as dam regulation and water diversion as well as natural factors such as monsoon climate often result in strong intra-annual variability in river discharge to the estuary (Carle et al., 2015; Wang et al., 2017; Gao et al., 2019). The unsteady river discharge alters estuarine hydrological regimes and further influences habitat conditions such as surface elevation and inundation at the marsh platform that are crucial for the establishment and survival of saltmarsh vegetation (Carle and Sasser, 2016; Brückner et al., 2019; Gao et al., 2019). Given the increasing variability of river discharge under intensified human activities and climate change, understanding its potential effects on estuarine saltmarsh vegetation thus becomes an imperative issue.

River mouth bar is a typical morphological unit formed at the estuary or delta front where saltmarshes similar to river-dominated tidal freshwater marshes often emerge (Twilley et al., 2019). For the vegetation in the proximal mouth bar area (i.e., the area facing the river), its direct exposure to flood during the high flow stage may influence its survival and growth through uprooting (Pasquale et al., 2014; Brückner et al., 2019). Whether the vegetation can survive or not depends on its resistance ability to flow impact at different growth stages (Brückner et al., 2019). In addition, the enhanced sediment deposition during the flood events may cause plant burial, especially for seedlings, and increase vegetation mortality (Sun et al., 2010). Indirectly and over

*Corresponding author. Tel.: +86 10 58805053.
E-mail address: ddshao@bnu.edu.cn (D. Shao).

*Corresponding author. Tel.: +86 10 58805053.
E-mail address: suntao@bnu.edu.cn (T. Sun).

ISSN: 1726-2135 print/1684-8799 online
 doi:10.3808/jei.202300498.

a larger time scale, flood also plays a critical role in shaping the river mouth bar geomorphology that provides the substrate for marsh colonization. While flood event could erode the main distributary channel at the proximal mouth bar zone (Carle et al., 2015), it was also found to increase sediment deposition at the middle and distal mouth bar zones (i.e., the area further offshore), creating new land for potential marsh colonization after the flood event (Cahoon et al., 2011; Carle et al., 2015; Twilley et al., 2019).

The response of marsh vegetation to unsteady river discharge has been explored in some recent studies. Based upon linear regression analysis, Kearney et al. (2011) found that there was no significant marsh coverage difference before and after diversion operations both at the Caernarvon diversion and control site in Louisiana, USA, due to limited sediment supply and excessive nutrient flux (Elsey-Quirk et al., 2019). Meanwhile, it was reported that the vegetated area in the Wax Lake Delta, a subdelta of the Mississippi River, increased in distal deltaic area after a historical flood event due to vertical accretion, whereas those in the directly downstream of the river mouth and along the main distributary channel experienced erosion (Carle et al., 2015). In addition, the increased discharge from April to September in 2016 significantly enlarged the available niches for pioneering marsh vegetation in the frontier mudflat area of Chongming Island, Yangtze River Estuary, China, resulting in a considerably greater rate of vegetation expansion in this wet year than previous normal years (Hu et al., 2019).

Regarding the effects of flood or unsteady river discharge on estuarine saltmarsh vegetation, clearly, contrasting observations were reported from the above studies in different sites (Caernarvon vs Wax Lake Delta vs Chongming Island) and even the different localities of the same site (proximal vs distal area). In viewing the varying direct and indirect impacts of flood on the saltmarsh vegetation and its habitat as well as the field evidence, we hypothesize that there are both positive and negative effects of unsteady river discharge on saltmarsh vegetation distribution. Specifically, on one hand, as a critical disturbance threshold is exceeded, strong flood disturbances during periods of high flow could result in immediate vegetation mortality. At the same time, big floods cause erosion and reduce habitable area at the proximal mouth bar zone. On the other hand, the extra sediment supply during flood events gradually increases elevation in distal area and creates new habitable area for vegetation colonization. The vegetation will colonize as long as external physical forcing is below critical disturbance threshold. The net effect of the trade-off between marsh expansion and erosion is both time- and space-dependent, and further depends on the timing, duration and magnitude of the high flow as well as the associated sediment supply.

Numerical models are increasingly applied to study saltmarsh distribution and development in estuarine zones (Huang et al., 2008; Ge et al., 2013; Best et al., 2018), which may assist in gaining understanding on the response of marshes to unsteady river discharge as they can isolate the relevant forcing factors and processes and quantify their effects. So far, a few studies have used a vegetation dynamics model which incorporates the ability of marsh vegetation in different growth phases to resist to external stress in tidal environments (Brückner et al., 2019; Odink, 2019). The response of saltmarsh vegetation to flow stresses in these studies was modelled through life-stage-dependent growth and mortality (Brückner et al., 2019). However, the existing modelling studies typically assumed a constant river discharge and neglected its intra-annual variability. As such, our understanding of the effects of unsteady river discharge on pioneer saltmarsh vegetation colonization and distribution is still limited.

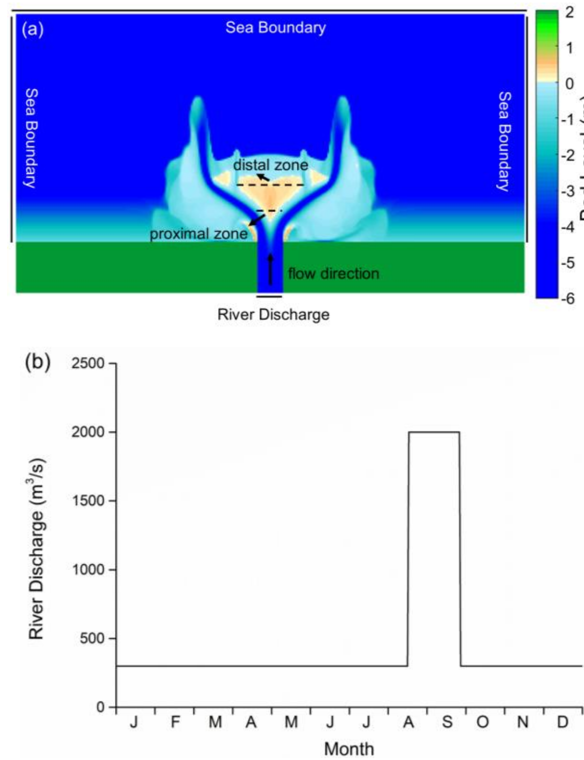

Figure 1. (a) The computational domain and the zonation of the initial mouth bar; (b) schematized unsteady river discharge at the upstream river boundary.

To address this gap and test our hypothesis on the trade-off effects of unsteady river discharge on saltmarsh vegetation colonization, this study aims to explore how high flow, which characterizes the intra-annual variation of the river discharge, affects vegetation colonization in a river mouth bar during the part of the plant life cycle when the plants are juvenile or mature, clonally spreading (Cui et al., 2009; Zhang et al., 2016). Numerical experiments were performed in Delft3D (Lesser et al., 2004) to simulate the evolution of a schematized river mouth bar under prototypical unsteady river discharge scenarios. The simulated hydrodynamic and morphodynamic changes were further used to drive a vegetation dynamics model developed based on the widespread Spartina alterniflora species in real time to model the resultant vegetation responses throughout the plant life history. Here, we focus on the mouth bar area as it has been proved as a 'hot spot' under the influences of river discharge and tides (Lera et al., 2019). In our study, the high flow could occur in summer due to monsoon, such as in Yangtze River (Hu et al., 2019), or in early spring due to rainfall and snowmelt, such as in Scheldt river (Smis et al., 2010) and many other European rivers (Szczypta et al., 2012). As our primary focus lies on the effects of unsteady river discharge on vegetation distribution, we adopted one-way approach to couple the hydro- and morpho-dynamics model with the vegetation dynamics model and did not consider the vegetation feedback.

According to our hypothesis, the following specific questions are addressed: (1) what are the spatial patterns of saltmarsh vegetation distribution in a river mouth bar under unsteady river discharge throughout the plant life cycle? (2) How does the vegetation distribution patterns relate to unsteady river discharge with different intra-annual variability, including the associated sediment supply? Answering the above questions could help advance our understanding on how estuarine saltmarshes as important coastal ecosystem responds to shifting hydrological regimes due to increasing human activities and climate change, and could also improve the operational strategies of water diversions in river deltas to restore coastal wetlands. The paper is organized as follows: the Delft3D model setting is described in Section 2.1, which is followed by the introduction of the unsteady river discharge scenarios in Section 2.2. The vegetation dynamics model, including the implementation of plant life cycle and windows of opportunity, is documented in Section 2.3. The model simulation and data analysis methods are introduced in Secions 2.4 and 2.5, respectively. Simulation results concerning the response of vegetation distribution to different unsteady river discharge scenarios (i.e., flow regimes) are presented in Section 3, followed by the relevant discussions in Section 4. Finally, the conclusions are drawn in Section 5.

2. Methods

In this study, we used Delft3D, which is a process-based numerical model that solves hydrodynamics, sediment transport and morphodynamics in a coupled fashion, to simulate the evolution of a schematized river mouth bar under prototypical unsteady river discharge scenarios with a single peak. The unsteady river discharge scenarios were parameterised using the Indicators of Hydrologic Alteration (IHA) framework commonly used in ecohydrology community (Ruth and Brian., 2007). Subsequently, a vegetation dynamics model based on the widespread Spartina alterniflora species was built to couple with the Delft3D model to explore the vegetation responses to unsteady river discharge throughout the plant life history.

2.1. Delft3D Model Setting

Here, we adopted a schematized river mouth bar as a representative river-dominated saltmarsh ecogeomorphological system for generic modelling purpose. An idealized geometry similar to Gao et al. (2019) was assumed. The computational domain (15,000 m × 7,500 m) was rectangular with a river channel cutting through the shoreline and flowing into the receiving basin (Figure 1a). The grid size in the central domain was 25 m × 25 m, and the grid size in the peripheral domain was 100 m × 100 m. The cross section of the initial river channel was rectangular and measured 400 m in width and 4 m in depth. The initial water depth was 4 m nearshore and increased seaward with a bed slope of 0.0035. The open boundaries included one upstream river boundary and three seaward boundaries. We specified the river discharge and sediment concentration at the upstream river boundary. For the seaward boundaries, fluctuating water level due to tides was prescribed at the one that was parallel to the shoreline, and zero lateral gradient in water level was imposed at the two lateral seaward boundaries. Simplified semidiurnal tides with a tidal range of 1 m was assumed in our simulations. The hydrodynamic time-step was set to 6 s to ensure simulation accuracy and stability. To save computing time, morphological acceleration factors of 20 and 120 were used during period of high and low flows, respectively. The values of morphological factor were determined by a series of sensitivity tests to attain the maximum values that ensure sufficient computational accuracy. The median sediment grain size is silt in many deltas, which could vary from 50 to 200 um (Caldwell and Edmonds, 2014; Ma et al., 2017). Therefore, a typical median sediment grain size of 90 um was chosen. Following Edmonds and Slingerland (2010) and Gao et al. (2018), the specific sediment density and dry bed density were set to 2,650 and 1,600 kg/m^3, respectively. The Chezy coefficient was fixed at 65 m$^{1/2}$/s (Zhou et al., 2014). Detailed information for the Delft3D model setting is documented in Table 1.

Table 1. Major Parameters of Delft3D Model

Modeling Parameter	Value	Unit
Cell size	25/100	m
Initial erodible sediment thickness	10	m
Initial bed slope	0.0035	°
Chezy coefficient	65	m$^{1/2}$/s
Sediment grain size	90	μm
Morphological acceleration factors	20/120	-
Hydrodynamic time-step	6	Second

2.2. Unsteady River Discharge Scenarios

We firstly ran a template scenario with a constant high flow running throughout an entire year to obtain the initial mouth bar as a basis for all subsequent unsteady river discharge scenarios. We adopted ranges of the river discharge, sediment load, and sediment grain size representative of the world's large rivers (Syvitski and Saito, 2007; Latrubesse, 2008). In this template scenario, the constant high flow, and sediment concentration were set to 2,500 m^3/s and the associated equilibrium sediment concentration. All unsteady river discharge scenarios were simulated from the initial mouth bar created by the template scenario. Following Gao et al. (2018, 2019), we adopted a simplified hydrograph with a stepped flood pulse, i.e., combination of constant low flow and high flow, to represent unsteady river discharge with intra-annual variability (Figure 1b). This simplification was justifiable as many rivers are with a single welldefined flood period (Szczypta et al., 2012; Gao et al., 2019). Here, we adopted three IHA indicators, namely, the magnitude of the high flow and low flow and the duration of high flow, to parameterise and construct the different unsteady discharge scenarios.

We designed two groups of scenarios with distinct timing

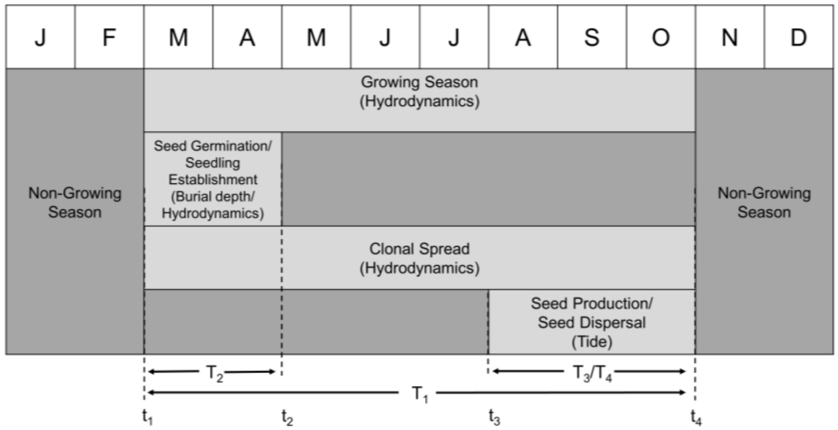

Figure 2. Plant life cycle of perennial herb marsh species and the key factors in each WoO.

of the high flow. For the first group, the onset of the high flow was set to 226th Julian day (August 15th), when the plants are mature and clonally spreading in mid-summer. This scenario is exemplified by the river discharge regime of Yellow River with natural seasonality and the added disturbance from the Water and Sediment Regulation Scheme (WSRS) (Wang et al., 2017). Alternatively, high flow usually occurs in winter or spring in many European rivers, such as Elbe River and Scheldt River (Szczypta et al., 2012; Wang et al., 2019). Further considering the growing season of saltmarsh vegetation, we chose the 76th Julian day (March 16th) when seeds started to germinate and plants were juvenile as the onset of high flow for the second group. The duration of the high flow for both groups can vary between 20 and 40 days (Gao et al., 2018). To ensure model stability, a transition period of two days with linearly varying discharge was chosen between low- and high-flow stages.

To explore unsteady river discharge with different intra-annual variability, we designed scenarios with different combinations of flow and sediment parameters. The high flows were set to 2,000 and 3,000 m^3/s, and the sediment concentrations were 0.5 and 2 kg/m^3. The river discharge was 300 m^3/s during the low flow period with an equilibrium sediment concentration, which was estimated by averaging sediment concentration at the inflow boundary from a model scenario with constant low flow occurring throughout an entire year. We did not change low flow condition in our scenarios, due to the limited changes in morphology during periods of low flow. The information for all scenarios is documented in Table 2.

2.3. Vegetation Dynamics Model

Most perennial herbaceous saltmarsh species, such as Spartina alterniflora, are important pioneer species, which play a key role in long-term ecogeomorphological evolution (Ge et al., 2015b). This kind of species usually has an ability in both fast-colonizing through seed dispersal and slow-colonizing through clonal spread (Ning et al., 2020). Here, we assumed a generic perennial herbaceous pioneer species based on S. alterniflora, which is a native species in the East Coast of North America and has spread to many parts of the world and is thus of global relevance (Zheng et al., 2018; Ning et al., 2021). In line with the life history and traits of S. alterniflora, our vegetation dynamics model consisted of several modules encompassing seed germination, clonal spread, seed dispersal and mortality. The framework of Window of Opportunity (WoO) was adopted to account for the responses of vegetation to unsteady river discharge in different plant growth stages, of which the relevant mechanisms have been well reported in the literature (Balke et al., 2014; Ge et al., 2015a; Brückner et al., 2019). It is also noted that salinity effect was neglected in our vegetation model. This is because only under the combination of infrequent inundation and intensive evapotranspiration, which usually occur in middle and high marshes, can salinity become a limiting factor for saltmarsh vegetation growth (He et al., 2009; Xue et al., 2017).

Table 2. Scenarios of Unsteady River Discharges in Delft3D Model

	Scenario	High Flow (m^3/s)	The Onset of High Flow (Julian Day)	Duration of High Flow (d)	Sediment Concentration (kg/m^3)
Group I	D1S1T1	2000	226	40	2
	D2S2T1	3000	226	40	0.5
	D2S1T1	3000	226	40	2
Group II	D1S1T2	2000	76	40	2
	D2S2T2	3000	76	40	0.5
	D2S1T2	3000	76	40	2

2.3.1. Plant Life Cycle and Window of Opportunity

Similar to Ge et al. (2015b), we divided the plant life cycle into four components, namely, seed germination, clonal spread, seed production and seed dispersal (see Figure 2). We set the phenological points (t_1, t_2, t_3, t_4) for each ecological process (T_1, T_2, T_3, T_4) and further used Boxcar function (Equation 1) to define its duration. The details of the various phenological points are documented in Table 3.

$$\prod_{t_m,t_n}(t) = H(t - t_m) - H(t - t_n) \quad (1)$$

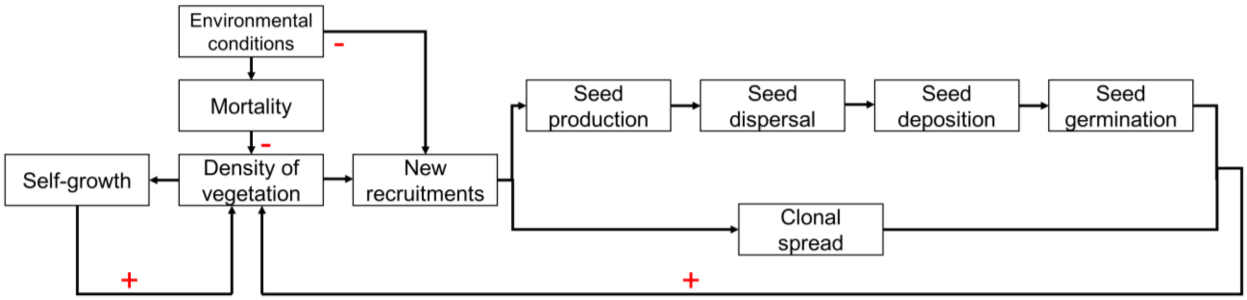

Figure 3. Model structure of marsh vegetation dynamics model. Note that +/– sign signifies positive/negative effect.

Table 3. Modelling Variables and Parameters of the Vegetation Dynamics Model

Variable	Description	Value	Unit	Reference
P	Plant population density	-	Number of shoots/m^2	
R_{ger}	Seed germination rate	-	Shoots/seeds	
R_{smor_v}	Mortality of seedling to velocity	-	%	
R_{smor_s}	Mortality of seedling to sediment deposition		-	
R_{amor_v}	Mortality of adult plant to velocity	-	yr^{-1}	
Eb	Seed burial depth	-	cm	
ΔE	Elevation change	-	m	
Parameters				
D	Diffusion coefficient of marsh vegetation	3	m^2 yr^{-1}	Xie, B.H., Personal communication, January 14, 2019
r	Growth rate of plant	0.05	yr^{-1}	Xie, B.H., Personal communication, January 14, 2019
C_{max}	Maximum plant density carrying capacity	200	Number of shoots/m^2	(Liu et al., 2014)
S	The number of seeds in seedbank	202	Number of seeds/(m^2.year)	(Xiao et al., 2009)
h_1	The threshold depth for seed germination	10	cm	(Deng et al., 2009)
h_2	plant height growth	0.01	m	Xie, B.H., Personal communication, January 14, 2019
v_{smax}	Velocity upper limit for linear seedling mortality range	0.4	m/s	(Brückner et al., 2019)
v_{smin}	Velocity lower limit for linear seedling mortality range	0.25	m/s	(Brückner et al., 2019)
v_{amax}	Velocity upper limit for linear adult mortality range	0.56	m/s	(Brückner et al., 2019)
v_{amin}	Velocity lower limit for linear adult mortality range	0.4	m/s	(Brückner et al., 2019)
t_1	Time of growing season and seed germination starting	61	-	(Ge et al., 2013)
t_2	Time of seed germination end	121	-	(Ge et al., 2013)
t_3	Time of seed production and seed dispersal starting	240	-	(Ge et al., 2013)
t_4	Time of seed production, seed dispersal, clonal spread as well as growing season end	304	-	(Ge et al., 2013)

where t_m and t_n are the respective phenological points of an ecological process expressed in Julian day, t is Julian day, and $H(t)$ is Heaviside step function. The Boxcar function assumes the value of 1 for $t_m \le t \le t_n$ and 0 otherwise.

WoO is widely used to hindcast and potentially predict colonization events in ecosystems where new establishment is disturbance limited (Balke et al., 2014), which was applied here to account for how unsteady river discharge affects marsh vegetation in each ecological process. Seed dispersal by tides is considered the main reproduction strategy for fast-colonizing pioneer marsh vegetation (Schwarz et al., 2018). Therefore, following Brückner et al. (2019), we assumed that all grids that were flooded and subsequently dried were designated as locations of seedbank. Seeds remained in the seedbank until next growing season arrived. Whether seeds can germinate in the following growing season depended on how much sediments deposited after seed dispersal. After seed germination, bed shear stress from tides and river flow is known as the main bottleneck for seedling establishment and adult plant growth on tidal flats (Barendregt and Swarth, 2013; Hu et al., 2015). Seedling can establish if bed shear stress and sediment deposition are below certain threshold (Sun et al., 2010; Brückner et al., 2019). Because of limited observational data on bed shear stress, we used depth-averaged grid velocity to replace bed shear stress to set the threshold of vegetation survival in our model.

2.3.2. Model Equations

The model structure is shown schematically in Figure 3. To simulate the spatio-temporal distribution of saltmarsh vegetation, the density of vegetation (number of shoots/m^2) was modelled by incorporating clonal spread, plant self-growth, seed germination and mortality (Takahashi et al., 2019). Marsh vegetation community consists of many circular colonies of various sizes, with their size increased by lateral clonal growth (Taylor et al., 2004; Takahashi et al., 2019). Diffusion equations have been successfully applied in simulating the lateral clonal spread of emerged (Yang et al., 2014) and submerged (Vilas et al., 2017) vegetation species. Therefore, we used diffusion term to simulate the clonal spread. Afterwards, vegetation grows slowly after it colonizes into a new region due to fewer propagules of limited population density (Taylor and Hastings, 2004). With population density growing, population growth rate decreases due to space limitations in the high-density meadow (Taylor et al., 2004). Therefore, we used logistic growth to model plant self-growth. The governing equation is as follows:

$$\frac{\partial P}{\partial t} = \prod\nolimits_{t_1,t_4}(t)\left[D\nabla^2 P + rP\left(1-\frac{P}{C_{\max}}\right)\right] + \prod\nolimits_{t_1,t_2}(t)R_{ger}\left(1-R_{smor\_v}\right)S\left(1-R_{smor\_s}\right) - PR_{amor\_v} \quad (2)$$

where P represents vegetation density (shoots/m^2), D represents clonal spread due to rhizome elongation (m·yr^{-1}), $\nabla^2 = (\partial^2 / \partial x^2) + (\partial^2 / \partial y^2)$ is the Laplacian operator, r is the maximum growth rate (yr^{-1}), C_{max} is the maximum density supported by the system (carrying capacity, number of shoots/m^2), R_{ger} is a switch that is either 0 or 1 depending on the burial depth (shoots/seeds), S is the number of seeds in seedbank after seed dispersal (number of seeds/(m^2·yr)), R_{smor_v} is the mortality rate of seedling under hydrodynamic stress (%), R_{smor_s} is the mortality rate of seedling under sediment deposition (%), R_{amor_v} is the mortality rate of adult plant under hydrodynamic stress (yr^{-1}), $rP[1 - (P / C_{max})]$ is the logistic growth term to simulate the population self-growth, $R_{ger}(1 - R_{smor\_v})S(1 - R_{smor\_s})$ is the survived seedling under the stress of hydrodynamics and sediment deposition, and PR_{amor_v} is the mortality of adult plants under hydrodynamic stress.

The seed density in seedbank grids assumed value from the literature (Xiao et al., 2009). We further assumed that the seedbank provided seeds for germination at a constant rate throughout the germination period. A few centimeters thick sediment layer might form after flooding and thus affects seed germination and seedling establishment due to lack of oxygen (Sun et al., 2010). Hence, we assumed that seeds only germinated below a threshold burial depth (see Equation 3), and burial depth was estimated from the elevation change in the non-growing season.

$$R_{ger} = \begin{Bmatrix} 1 & E_b \le h_1 \\ 0 & \text{Otherwise} \end{Bmatrix} \quad (3)$$

where E_b is seed burial depth (m), and h_1 is the threshold depth for seed germination (m).

After seeds germinate, the most vulnerable stage arrives. The seedlings will be uprooted if the flow velocity is greater than their tolerated level. During the seedling establishment stage (from t_1 to t_2), a linear dose-effect relation in which the mortality rate increases with increasing pressure was used to calculate the mortality caused by hydrodynamic stress (Brückner et al., 2019) (see Equation 4). When the plants grew into adult stage (from t_2 to t_4), another threshold with linear dose-effect relation was used for calculating adult plant mortality (see Equation 5). In addition, we assumed that if the elevation change (ΔE) exceeds plant height growth (h_2), the seedlings were unable to survive (Brückner et al., 2019) (see Equation 6).

$$R_{amor\_v} = \begin{cases} 0 & \text{if } v \le v_{amin} \\ (v - v_{amin})/(v_{amax} - v_{amin}) & \text{if } v_{amin} < v \le v_{amax} \\ 0.1 & \text{if } v > v_{amax} \end{cases} \quad (4)$$

$$R_{smor\_v} = \begin{cases} 0 & \text{if } v \le v_{smin} \\ (v - v_{smin})/(v_{smax} - v_{smin}) & \text{if } v_{smin} < v \le v_{smax} \\ 0.3 & \text{if } v > v_{smax} \end{cases} \quad (5)$$

$$R_{amor\_v} = \begin{cases} 0 & \text{if } v \le v_{amin} \\ (v - v_{amin})/(v_{amax} - v_{amin}) & \text{if } v_{amin} < v \le v_{amax} \\ 0.1 & \text{if } v > v_{amax} \end{cases} \quad (6)$$

where v is depth-averaged grid velocity (m/s); v_{smax} is the velocity upper limit for linear seedling mortality range (m/s); v_{smin} is the velocity lower limit for linear seedling mortality range (m/s). v_{amax} is the velocity upper limit for linear adult mortality range (m/s); v_{amin} is the velocity lower limit for linear adult mortality range (m/s), h_2 is the plant height growth (m), ΔE is elevation change (m). The parameters of the vegetation dynamics model assumed ranges of value reported in the literature and from personal communications wherever possible. Detailed information of all modelling variables and parameters are provided in Table 3.

2.4. Simulation of Coupled Ecogeomorphological Model

Before all formal scenario simulations, we ran a prelimnary simulation to obtain initial vegetation distribution. Specifically, the results of the template hydro- and morphodynamics simulation were used as the initial condition to feed the vegetation dynamics model, and we started with the assumption that all cells above 0 m in the initial mouth bar formed were covered by vegetation (Li et al., 2018). We further used the resultant vegetation distribution to run one year simulation of both Delft3D and the vegetation dynamics model, assuming that high flow (2,500 m^3/s and equilibrium sediment concentration) occurred from 226th Julian day (August 15th) and lasted for 40 days when plants were mature and clonally spreading in mid-summer. The vegetation density and seed bank distribution obtained at the end of the growing season was adopted as the initial vegetation distribution for all subsequent unsteady flow scenarios.

The coupling time interval for the two models was one day, and the outputs of Delft3D simulation (bed level, water depth, land/sea boundary and velocity) during this interval were time-averaged and fed as input for vegetation dynamics model. The flowchart of the modelling approach is shown in Figure 4.

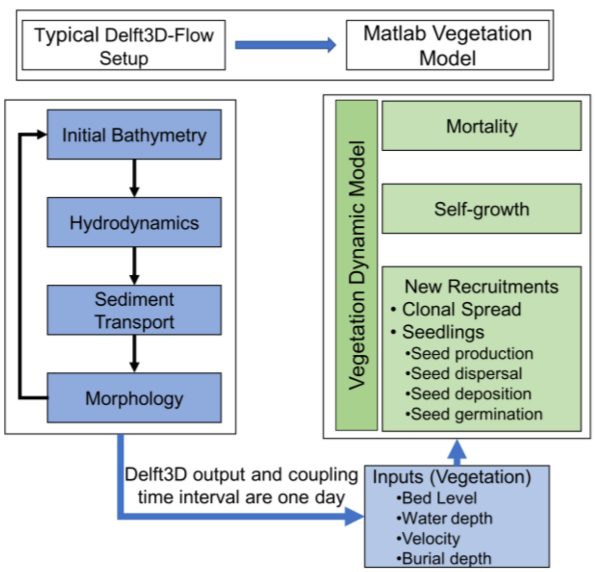

Figure 4. Flowchart of modelling approach (adapted from Best et al. (2018)).

2.5. Analyses of Numerical Results

The effects of unsteady river discharge on marsh vegetation spatial distribution were examined at the key time nodes during the growing season, including the onset of high flow, the end of high flow, and the end of the growing season. Following (Ge et al., 2015b), a grid was considered to be occupied by vegetation when vegetation density exceeded 2/3 of maximum capacity. The number of vegetated grids at the end of the growing season was counted and compared with that at the onset of high flow. Vegetation density change at the different mouth bar zones was also examined to better understand the spatial dependence of the vegetation response to the unsteady river discharge.

In this study, current velocity and sediment deposition are two key stressors controlling vegetation distribution (Equations 4 ~ 6). Therefore, we adopted normalized cross-section averaged velocity v^* and relative sediment concentration S^* at the river outlet as proxies of the "velocity" and "sedimentation" stresses to evaluate the vegetation response to unsteady river discharge:

$$v^* = (v - v_{amin})/(v_{amax} - v_{amin}) \tag{7}$$

$$S^* = S/S_e \tag{8}$$

where v is cross-section averaged velocity at river outlet during the period of high flow (m/s). S and S_e are sediment concentration (kg/m^3) and equilibrium sediment concentration (kg/m^3), respectively, at the river outlet during the period of high flow.

3. Results

3.1. The Effects of Unsteady River Discharge on Hydrodynamics and Geomorphology

Figure 5 shows the representative hydrodynamics simulation results on 230th Julian day (mid-summer, high flow stage) after the short transition period. The corresponding geomorphological changes before and after the high flow are presented in Figure 6. For the scenario with relatively low river discharge (D1S1T1), velocity decreases with distance from the river outlet (Figure 5b), and there is no significant change in elevation in the mouth bar zone before and after the high flow (Figure 6 a). In contrast, velocity is much greater at the proximal part and two flanks of the mouth bar for the relatively high discharge scenarios (D2S2T1 and D2S1T1, see Figures 5c ~ 5d). In such cases, geomorphological changes vary with varying sediment concentration. For the scenario with relatively low sediment concentration (D2S2T1), high flow seriously erodes proximal part and both flanks of the mouth bar (Figure 6b). However, the elevation in the center of the mouth bar increases slightly after the high flow. On the contrary, for the scenario with relatively high sediment concentration (D2S1T1), high flow carries extra sediment load and leads to mouth bar accretion and expansion (Figure 6c). Notably, newly created subaerial area is found in distal mouth bar zone in both scenarios with relatively high river discharge.

3.2. Vegetation Density Before and After High Flow

Figure 7 shows the vegetation density for the various scenarios on the 266th Julian day when high flow ends. Our simulation results show that the vegetation response varies significantly among the different scenarios. For the relatively low discharge scenario (D1S1T1), we found a steady decrease of vegetation density when approaching the mouth bar front (Figure 7b). This indicates that high flow causes strong damaging effects on the vegetation density in the proximal mouth bar zone. We attribute this type of marsh erosion to the drag force induced by flood (Type I) (Figure 5b). Alternatively, for the scenario with relatively high discharge and low sediment concentration (D2S2T1), shrinking in vegetated area is noted at both flanks of the mouth bar during the high flow stage (Figure 7c). We attribute this type of erosion to substrate erosion combined with the drag force (Type II) (Figures 5c and 6b). While for the scenario with relatively high discharge and high sediment concentration (D2S1T1), the lateral extent of the mouth bar significantly increases during the high flow stage (Figure 6c). However, the vegetation density in the newly created land is still low at the end of the high flow stage (Figure 7d) due to the pressure from high velocity (Figure 5d). It suggests that hydrodynamic force is still the dominant force in controlling vegetation distribution and expansion in such cases. Besides, vegetation density in the central and distal mouth bar zone is highest for the relatively high velocity scenarios, which is consistent with the locally reduced hydrodynamic pressure largely due to the higher elevation (Figures 5c ~ 5d).

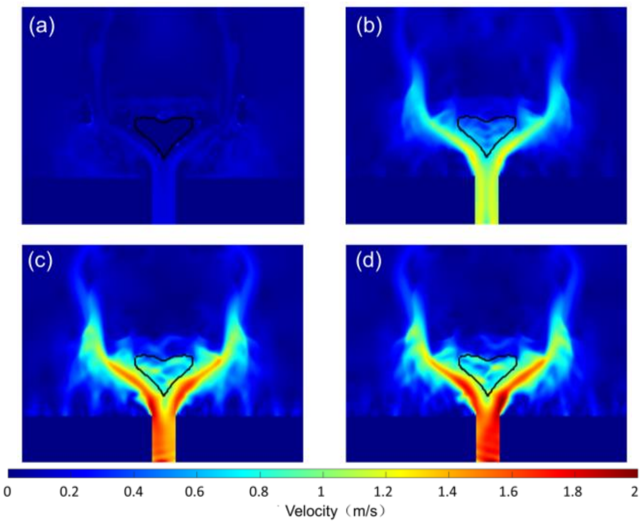

Figure 5. Comparison of velocity field before high flow (a) and that during high flow period (230th Julian day) for different scenarios: (b) D1S1T1, (c) D2S2T1, and (d) D2S1T1. The black line indicates the mouth bar outline before high flow stage.

3.3. The Evolution of Vegetated Area and Mouth Bar Area

The evolution of the vegetated area and subaerial mouth bar area (elevation > 0 m) over time for all scenarios with high flow occurring from the 226th Julian day is shown in Figure 8a. The vegetated area increases at the beginning of the seedling stage, which can be attributed to plant clonal reproduction resulting from sparsely distributed cells and colonization by seedling recruitment. The vegetated area reaches its maximum in mid-growing season and remains unchanged until high flow occurs as all suitable area of the mouth bar are fully occupied by the vegetation at this stage. Strong vegetation mortality occurs after the onset of the high flow, leading to immediate decline of the vegetated area. As the high flow ends, the vegetated area grows back and the recovery continues for a while in the subsequent low flow stage. As expected, the decline is minimal for the relatively low (discharge) velocity scenario (D1S1T1). For the more severely affected relatively high (discharge) velocity scenarios, the vegetated area at the end of the growing season does not recover the level before the decline for the low sediment concentration scenario (D2S2T1). This suggests that the vegetated area gained at the distal mouth bar zone is unable to compensate the eroded vegetated area due to Type II erosion at the two flanks of the river mouth (Figures 6b and 7c). On the contrary, the vegetated area significantly increases after the high flow stage and eventually exceeds the level before the decline for the high sediment concentration scenario (D2S1T1). This is mainly due to the vegetation expansion into the considerable newly created land across the whole mouth bar (Figures 6c and 7d). The contrast between the various scenarios also indicates the trade-off effects of the high flow on the marsh vegetation.

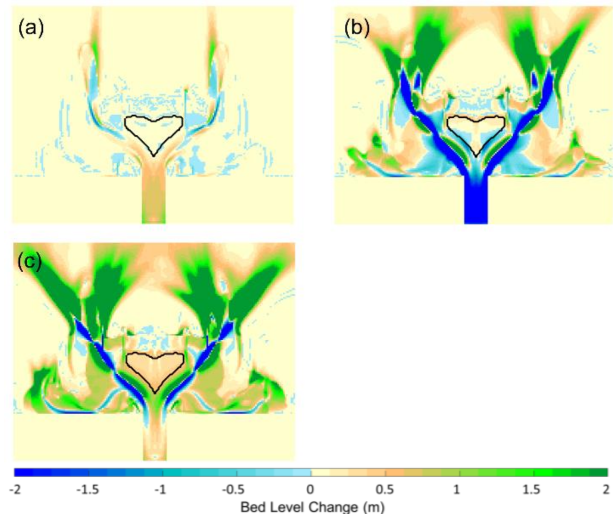

Figure 6. Comparison of elevation changes after high flow between different scenarios: (a) D1S1T1; (b) D2S2T1; and (c) D2S1T1. The black line indicates the mouth bar outline before high flow stage.

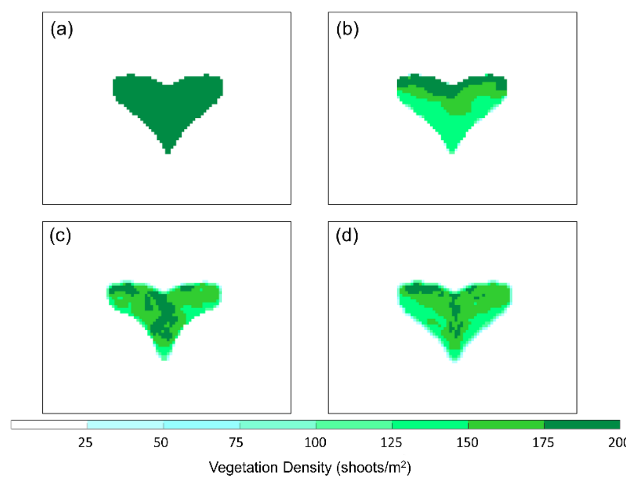

Figure 7. Comparison of vegetation density before high flow (a) and that after high flow for different scenarios: (b) D1S1T1, (c) D2S2T1, and (d) D2S1T1.

Our numerical results show that the evolution of the vegetated area is also related to that of the subaerial mouth bar area. Before the high flow strikes, the two areas are identical because all suitable area of the mouth bar are almost fully occupied by the vegetation. During the high flow, vegetated area drops more significantly for both relatively high discharge scenarios (D2S2-

T1 and D2S1T1), suggesting that both Type I and Type II erosions contribute to marsh erosion. After the high flow, the vegetated area grows back with the growing subaerial mouth bar area, and the two areas gradually match again at the end of the growing sea, except for the scenario with relatively high discharge and high sediment concentration (D2S1T1). This is because the termination of the vegetation growth leaves no chance for further vegetation expansion into the large remaining newly created land.

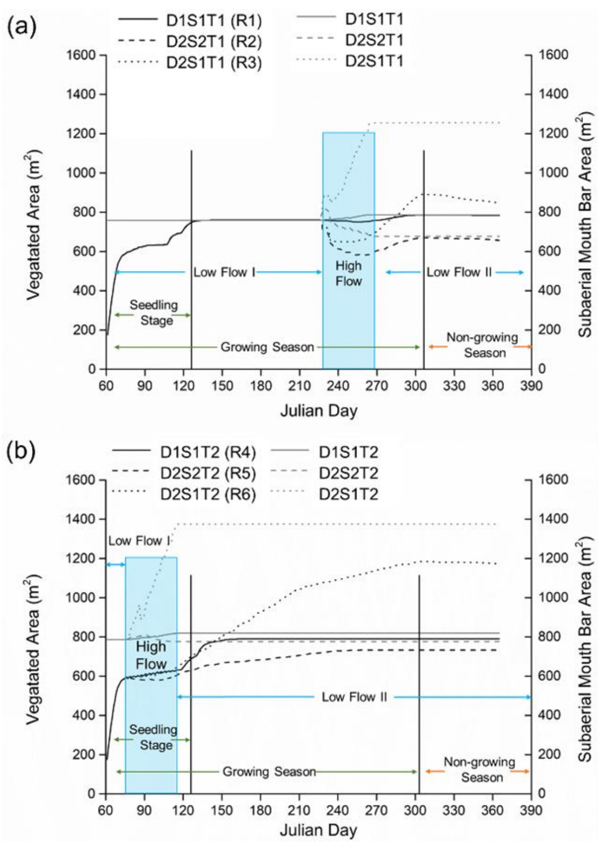

Figure 8. Evolution of vegetated area and subaerial mouth bar area (> 0 m) over time. (a) when high flow occurs from 226th Julian day (mid-summer); (b) when high flow occurs from 76th Julian day (early spring). The black lines indicate vegetated area, the grey lines indicate mouth bar area.

3.4. Regimes of Vegetation Response to Unsteady River Discharge

Based on the simulated spatial variations of vegetation distribution and density as well as the vegetated area throughout the whole growing season presented above, the vegetation response is subject to the trade-off between vegetation expansion and erosion induced by unsteady river discharge, particularly the dominant high flow stage. The overall effect of the trade-off can be summarized by three different regimes defined on the parameter space of normalized velocity and sediment concentration metrics (Equations 7 and 8) during the period of high flow and at the river outlet (see Figure 9). The three vegetation response regimes are described as follows:

R1. Minimal impact with small flood. Relatively low discharge during the period of high flow has little direct impact on the plants, and the flood-induced erosion of the mouth bar is also relatively low.

R2. Erosion with big flood and low sediment supply. Relatively high discharge during the period of high flow causes significant damage on the plants (e.g., uprooting) due to the flood-induced drag force, and also causes significant erosion at the proximal part and both flanks of the mouth bar due to limited sediment supply. Marsh recovery is incomplete after the high flow.

R3. Expansion with big flood and high sediment supply. Flood-induced drag force causes the same damage on the plants, but due to sufficient sediment supply, net accretion, and expansion occurs at the mouth bar, allowing marsh expansion after the high flow.

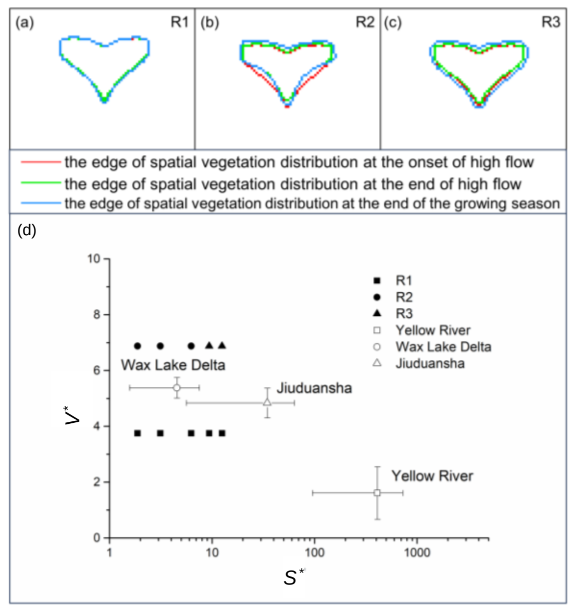

Figure 9. Responses of vegetation to unsteady river discharge. (a) ~ (c) spatial vegetation distribution patterns in response to different unsteady river discharge scenarios when high flow occurs from the 226th Julian day. Red line, green line and blue line represent the edge of spatial vegetation distribution at the onset of high flow, the end of high flow as well as the end of the growing season, respectively. (d) Distribution of the three regimes on V^* vs S^* space. V^* and S^* are normalized cross-section averaged velocity and relative sediment concentration, respectively.

4. Discussion

4.1. The Trade-Off Effect of Unsteady River Discharge on Vegetation Distribution

Our results indicate that there is trade-off effect of unsteady river discharge on vegetation distribution. Negative effects are observed through the response of vegetation to flood in the proximal part and two flanks of the mouth bar. When high flow occurs from the 226th Julian day (mid-summer), the seedlings have already grown into mature plants and developed a strong root system to increase their tolerance to flow impact and prevent severe damages such as uprooting (Cao et al., 2018). This is parameterized by the seedling and adult life-stage in our model (Equations 4 and 5). Despite the tolerance to velocity, high flow can still cause negative effects on vegetation and lead to marsh erosion at the proximal part and two flanks of the mouth bar. Similarly, Carle et al. (2015) reported that in Wax Lake Delta, vegetated area directly downstream of the river mouth and along the main distributary channel experienced erosion.

Our results also indicate that the negative effects are strongly spatially dependent and dictated by the spatially varying flow velocity and elevation (Figures 5b ~ 5d and Figures 6a ~ 6c). The spatially varying effects are also observed in river sand bar or gravel bar, where vegetation is subject to flood disturbance as well (Caponi et al., 2019; Wintenberger et al., 2019). Wintenberger et al. (2019) demonstrated that vegetation in fixed sand bar area, which is characterized by minor morphological changes, is more susceptible to Type I erosion, whereas vegetation in eroded area, where sedimentary processes are intense, is more prone to Type II erosion. Similarly, our simulation results show that floods significantly increase flow velocity for the majority of the mouth bar area (see Figures 5b ~ 5d). This leads to immediate vegetation erosion directly downstream of the river mouth due to flood-induced drag force (Type I). When high flow ends, vegetation is able to recover and occupy the proximal mouth bar zone as long as the reduced flow disturbance is below its survival threshold (Figure 8a). At the same time, vegetation at the two flanks of the mouth bar can be eroded if the high flow is relatively high and the carried sediment concentration is relatively low (Figure 7c), which is irreversible because the erosion occurs to the mouth bar as the substrate for the vegetation colonization (Figure 6c), i.e., the Type II erosion.

The positive effects of high flow arise from extra sediment delivery. Most sediments are delivered into coastal bays and the inner shelf during the high flow stage, and then reworked by tides or waves, leading to sediment deposition at distal mouth bar area and thus vertical and horizontal accretion (Twilley et al., 2019; Liu et al., 2021) (see Figures 6b ~ 6c). New land created through accretion during the high flow stage provides an opportunity for vegetation expansion after the high flow (Figures 8a and 9c). Notably, when the high flow is relatively high, we found that the trade-off effect is highly dependent on the associated sediment concentration. At the proximal part and both flanks of the mouth bar, increasing sediment concentration transforms geomorphological changes from erosion to accretion. The dominant erosion force is also shifted from Type II to Type I. The geomorphological change eventually leads to net vegetation expansion and a regime shift from R2 to R3.

4.2. The Effects of Timing of High Flow

To test how timing of the high flow affects vegetation response, we ran another group of scenarios (Group II) assuming that high flow occurs in winter or spring, as in many European rivers such as Elbe River and Scheldt River (Szczypta et al., 2012; Wang et al., 2019). Further considering the growing season for saltmarsh vegetation, we chose the 76th Julian day (March 16th) when seeds started to germinate and plants were juvenile as the onset of the high flow. As shown in Figure 10, the overall patterns of the vegetation distribution of Group II scenarios are similar to those of Group I. The major difference is that the proximal mouth bar has not been fully occupied by vegetation when the high flow is shifted to early spring. Figure 8b shows that the shift of high flow to the seedling stage does hamper the seedling establishment and vegetation expansion, particularly for the scenario with relatively high discharge and low sediment concentration (D2S2T2). In contrast, vegetation expansion continues through the seedling stage without flow stress for all Group I scenarios (Figure 8a). For Group II scenarios, high velocity at the proximal mouth bar area persists during the high flow stage, preventing seedling establishment by directly imposing drag on the seedling (Equation 5) until high flow ends.

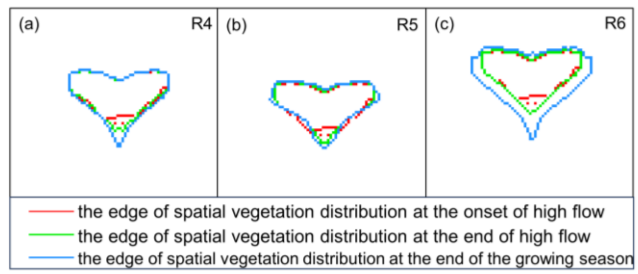

Figure 10. Spatial vegetation distribution patterns in response to different unsteady river discharge scenarios when high flow occurs from the 76th Julian day. Red line, green line and blue line represent the edge of spatial vegetation distribution at the onset of high flow, the end of high flow as well as the end of the growing season, respectively.

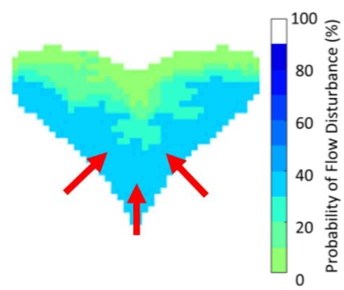

Figure 11. The spatial distribution of probability of flow disturbance of R4 during the high flow stage

As suggested by Hu et al. (2015), a sufficiently long disturbance-free period during seedling stage is the key for the occurrence of colonization events. The growth of seedling also requires a disturbance-free period so that their root can withstand the flow (Balke et al., 2011). The probability of flow disturbance was calculated by dividing the number of days when flow velocity was below velocity threshold by the duration of high flow. Figure 11 shows that the central mouth bar zone with higher elevation tends to have a larger probability in having a long enough disturbance-free period. Besides, the distal mouth bar zone tends

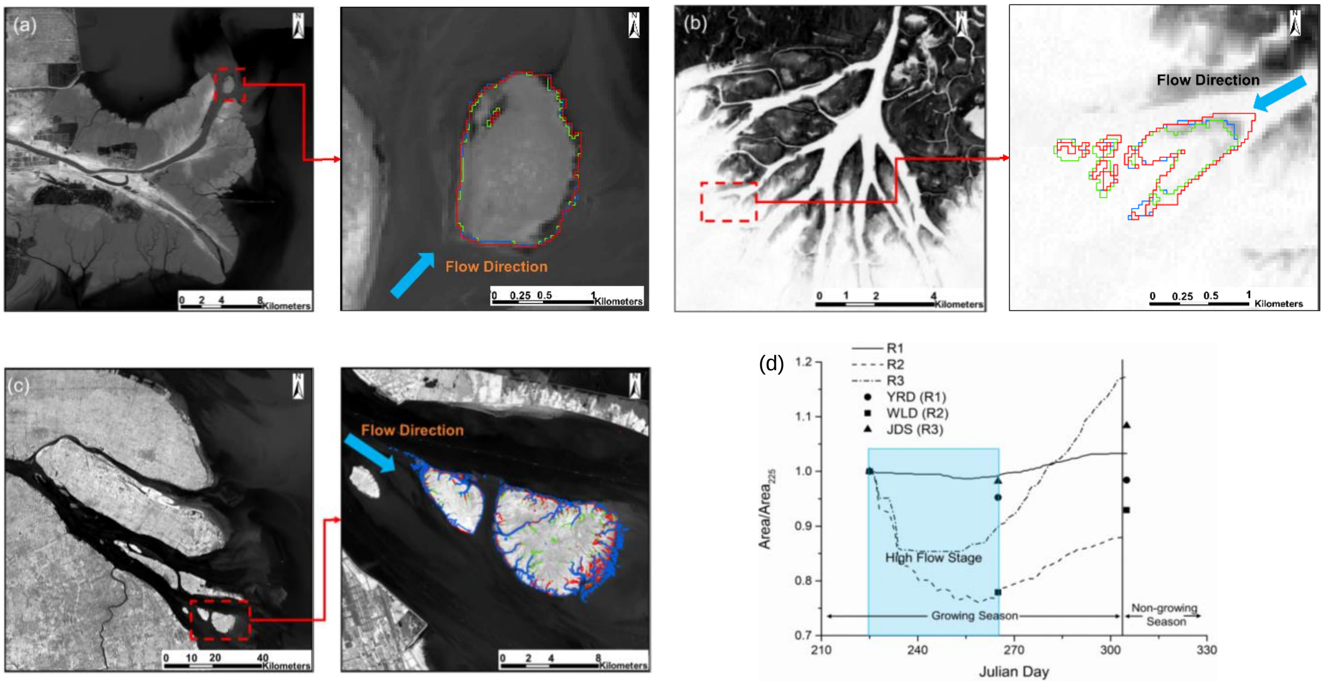

Figure 12. Comparisons of vegetated area before and after high flow: (a) ~ (c) location of the mouth bar and vegetation distributions in different time nodes during the growing season. (a) ~ (c) are mouth bar at the Yellow River Estuary (YRE), Wax Lake Delta (WLD), and the Jiuduansha Shoals (JDS), Yangtze River Estuary, respectively. Red line, green line and blue line represent the edge of spatial vegetation distribution before and after high flow period, as well as end of the growing season, respectively. (d) comparison of relative vegetated area between generic model simulation and real cases.

to experience long disturbance-free period as predicted by our hydrodynamics simulation (Figure 5). Less disturbance in the distal mouth bar zone results in lower vegetation loss during the high flow period (Figures 10b ~ 10c). Similar phenomenon was observed in the Wax Lake Delta (Carle et al., 2015). Vegetation was eroded in the proximal mouth bar zone in the historyical 2011 Mississippi River flood, whereas lower erosion occurred in the middle and distal mouth bar area.

Even though the timing of the high flow is vastly different, the vegetated area at the end of the growing season does not differ significantly between the Group I and II scenarios, except for the scenarios with relatively high velocity and high sediment concentration (R3 vs R6). Although both scenarios create almost equal amount of new land due to the high flow, the onset of the high flow in mid-summer results in shorter remaining growing season (40 days for R3 vs 190 days for R6) for subsequent vegetation expansion to newly created land. Moreover, when high flow occurs in the seedling stage, the flood affects less vegetated area and the affected seedlings can revive after a shorter recovery time (see Figure 8b). In such case, the timing of the high flow affects the ultimate saltmarsh extent.

4.3. Verification with Real Cases

In this study, we developed a vegetation dynamics model based on perennial herbaceous saltmarsh species *S. alterniflora*, and further coupled with Delft3D model to investigate how unsteady river discharge affected marsh vegetation. Our model successfully reproduces the well-established vegetation expansion pattern (see Movie S1). The short-distance vegetation expansion is characterized by a number of clonal propagules that are able to expand laterally, resulting in a single large patchy vegetation pattern (Schwarz et al., 2018). The long-distance vegetation expansion is characterized by small patchy vegetation pattern which is far away from its original community (Ge et al., 2015b). Separated vegetation patch are connected through clonal spread ing, and are eventually combined into one continuous vegetation patch (Taylor et al., 2004).

We further analyzed the response of vegetated area to unsteady river discharge in three natural mouth bar cases using the same methods presented in Section 2.5. Moreover, the relative vegetated area for three key time nodes, namely, before high flow, after high flow and at the end of the growing season, were calculated as well (see Supplementary Material for details). In principle, the three chosen cases verify the vegetation response regimes we proposed above. Specifically, for R1 (relatively low discharge), which is exemplified by the mouth bar at the Yellow River Estuary (YRE), both vegetation distribution and area change little before and after the high flow stage (Figures 12a and 12d). For cases with relatively high discharge and low sediment concentration, such as the Wax Lake Delta (WLD) (Figure 12b), vegetation erodes at the proximal and both flanks of the mouth bar during the high flow stage (Shaw et al., 2013; Carle et al., 2015; Olliver et al., 2020), resulting in significant marsh erosion. The subsequent recovery, albeit incomplete, is also well captured. For R3 (relatively high discharge and high sediment concentration), which is exemplified by the Jiuduansha Shoals (JDS) at the Yangtze River Estuary (Guo, 2013) (Figure 12c). Vegetation experiences minor erosion during the high flow period, and expands throughout the whole mouth bar area after the high flow, resulting in increased vegetated area at the end of the growing season.

In summary, the vegetation response to unsteady river discharge is dictated by the overall effect of the trade-off between expansion and erosion, which further depends on the timing, magnitude and duration of the high flow as well as the carried sediment concentration. This is illustrated in the conceptual diagram shown in Figure 13. In relatively low flow velocity condition, vegetation tends to remain in a stable condition, due to limited hydrodynamic pressure and geomorphological change (light green area in Figure 13). This can be observed from Yellow River Estuary (Figure 12a). In relatively high flow condition with low sediment concentration (dark yellow in Figure 13), vegetation erosion is primarily caused by Type II erosion. Therefore, it is unable for the vegetated area to recover to the level before the high flow. Such phenomenon is observed in the proximal mouth bar zone in Wax Lake Delta (Figure 12b). However, there are still chances for vegetation to grow back as long as the sediment supply is abundant. The sediment concentration can reverse the trade-off effect in relatively high velocity condition (blue arrow). In such condition, the vegetation erosion induced by Type I erosion is reversable as long as enough growing season remained in low flow stage (Figures 8, R3 vs R6). This can be observed at the Jiuduansha Shoal, Yangtze River Estuary (Figure 12c), where vegetation erodes slightly during the high flow stage, recovers after the high flow and ultimately attains a larger vegetated area at the end of the growing season.

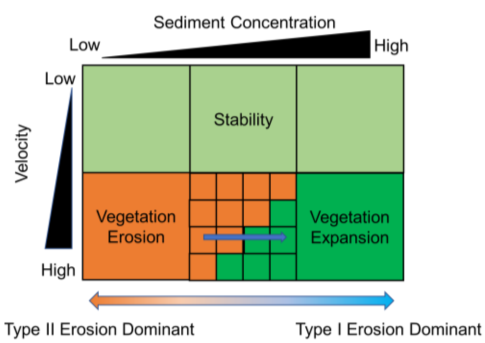

Figure 13. Conceptual model on how trade-off between river velocity and sediment concentration variation is affecting vegetation development at a river mouth bar.

4.4. Implications for Wetland Restoration

The fate of many deltaic floodplains relies on the sediment supply in combating wetland loss and degradation (Hiatt et al., 2019). Almost all sediments in the deltaic zone come directly or indirectly from rivers. In this context, restoration and regulation schemes such as water diversion and WSRS are considered the most effective tools for deltaic floodplain and wetland restoration. In order to maximize restoration goals, the sediment load and flood timing should be properly designed and optimized in a restoration project.

Based on the trade-off effects demonstrated in our study, we emphasize the importance of sediment supply with the river discharge in maintaining the stability of the ecogeomorphological system. The sediment concentration can shift the trade-off effect in relatively high velocity condition. In relatively high velocity with high sediment concentration condition, high flow could lead to vegetation loss due to Type I and Type II erosion but will eventually lead to net vegetation gain once it ends (Figure 8, R3 and R6). On the contrary, insufficient sediment supply results in veg- etation loss in the end. The important role of sediment in wetland restoration is well reported in the literature (Ezcurra et al., 2019; Ganju, 2019; Ladd et al., 2019; Liu et al., 2021), and a unsuccessful wetland restoration project at the Caernarvon diversion site also proved that extra freshwater with limited sediment supply contributed little to wetland restoration (Elsey-Quirk et al., 2019). Therefore, we emphasize that enough sediment supply should be considered when diversion project is conducted.

Another important issue on diversion management is how to minimize the negative effect of short-term flood pulse in causing vegetation loss while maximizing long-term wetland gain. The timing of the high flow can make a difference as demonstrated by our scenario simulations. Amongst other factors, the timing of the high flow relative to the plant life history determines the tolerance of the plant to the stress and thus its response, as well as the remaining period of the growing season and thus the duration of vegetation recovery after the high flow. Based on our simulation results, it is preferable to conduct water diversion in early growing season so that less vegetation will be influenced and longer vegetation recovery will be allowed. Similar strategyies were put forward by Peyronnin et al. (2017) that diversion during winter months could achieve better wetland restoration outcome through land building and preventing vegetation loss from prolonged and continuous flooding as plants are in the dormant state.

River mouth bar is widely recognized as a key morphological unit formed at the estuary or delta front that is subject to intense terrestrial and marine forcing, including river discharge, waves and tides, giving rise to complex depositional patterns. For example, in tide-dominated system, mouth bars are characterized by trifurcations rather than a wide mouth bar in river-dominated system (Leonardi et al., 2013), and vegetation is regularly influenced by daily to fortnightly variations in the tide and annual water level variations (Suchrow and Jensen, 2010), resulting in distinct geomorphology and hence the vegetation distribution. In wave-dominated system, extra wave-induced bed shear stress can be important for the morphodynamics of the mouth bar (Gao et al., 2018), as well as seeding establishment (Hu et al., 2015; Brückner et al., 2019). Further research can be extended to these tide/wave-dominated systems.

In addition, biotic feedbacks can be taken into consideration in future studies. Stabilization arises from below ground roots that can withstand higher tensile stresses and increase material strength and from dense aboveground biomass that diminishes turbulent kinetic energy in the flow, thereby increasing deposition and reducing sediment erosion (Fagherazzi et al., 2015). As suggested by Nardin and Edmonds (2014), wetlands in the proximal delta behave differently from that in the distal delta zone in how biotic feedbacks influence sedimentation as a function of vegetation height and density. Developing an ecogeomorphological model that considers the interacttions between vegetation, hydrodynamics and geomorphology in a two-way coupling fashion can provide a more comprehensive understanding on how the system evolves under environmental changes such as altering river discharges.

5. Conclusions

In this study, numerical experiments were performed using an ecogeomorphological modelling approach through the coupling of an in-house vegetation dynamics model and the hydro- and morphodynamics model Delft3D, to study the responses of vegetation to unsteady river discharge throughout the plant life history. Delft3D was used to simulate the evolution of a schematized river mouth bar under prototypical unsteady river discharge scenarios. The simulated hydrodynamic and morphodynamic results were further used to drive the vegetation dynamics model developed based on the Spartina alterniflora species with global relevance to simulate the response of spatio-temporal vegetation distribution to different unsteady river discharge scenarios.

Our results show that: 1) the imposed seasonal high flow can create more potential suitable habitat for the vegetation expansion and at the same time, cause erosion of vegetation through flood-induced drag force (Type I) as well as substrate erosion (Type II); 2) The net overall effect of the trade-off between expansion and erosion depends on the timing, magnitude and duration of the high flow as well as the carried sediment concentration, leading to three vegetation response regimes defined on the parameter space of normalized velocity and sediment concentration metrics, namely, minimal impact with small flood (R1), erosion with big flood and low sediment supply (R2), expansion with big flood and high sediment supply (R3); 3) the timing of the high flow determines whether the vegetation has enough time to occupy the newly created land at the rejuvenation stage after the high flow and thereby affects the overall saltmarsh extent; and 4) The three vegetation response regimes are verified in principle by observed flood-induced vegetation changes in real cases such as mouth bars at the Yellow River Estuary, Wax Lake Delta, and the Jiuduansha Shoal at the Yangtze River Estuary. Our results have important implications for understanding how saltmarsh vegetation respond to unsteady river discharge, and how to protect and restore them under intensive human activities and climate change.

Acknowledgments. This work was supported by the National Key R&D Program of China (grant 2019YFE0121500), the Joint Funds of the National Natural Science Foundation of China (grant U1806217), Key Project of the National Natural Science Foundation of China (grant 51639001), and the Interdisciplinary Research Funds of Beijing Normal University. W. Gao acknowledged support from the fellowship of China Postdoctoral Science Foundation (grant 2020M680438). W. Gao acknowledges support from the Young Scientists Fund of National Natural Science Foundation of China (grant 52101297) and the Fellowship of China Post-doctoral Science Foundation (grant 2020M680438). We gratefully acknowledge L. M. Sun for her valueble assistance in remote sensing interpretation. We are very thankful for the dedicated and patient guidance from Matthew P. Adams and Kate O'Brien on vegetation dynamic model.

References

Balke, T., Bouma, T.J., Horstman, E.M., Webb, E.L., Erftemeijer, P.L. A. and Herman, P.M.J. (2011). Windows of opportunity: thresholds to mangrove seedling establishment on tidal flats. *Mar. Ecol. Prog. Ser.*, 440, 1-9. https://doi.org/10.3354/meps09364

Balke, T., Herman, P.M.J. and Bouma, T.J. (2014). Critical transitions in disturbance-driven ecosystems: identifying Windows of Opportunity for recovery. *J. Ecol.*, 102, 1356-1356. https://doi.org/10.1111/1365-2745.12241

Barbier, E.B., Koch, E.W., Silliman, B.R., Hacker, S.D., Wolanski, E., Primavera, J., Granek, E.F., Polasky, S., Aswani, S., Cramer, L. A., Stoms, D.M., Kennedy, C.J., Bael, D., Kappel, C.V., Perillo, G.M.E. and Reed, D.J. (2008). Coastal ecosystem-based management with nonlinear ecological functions and values. *Science*, 319 (5861), 321-323. https://doi.org/10.1126/science.1150349

Barendregt, A. and Swarth, C.W. (2013). Tidal Freshwater Wetlands: Variation and Changes. *Estuar. Coast.*, 36, 445-456. https://doi.org/10.1007/s12237-013-9626-z

Best, Ü.S.N., Van der Wegen, M., Dijkstra, J., Willemsen, P.W.J.M., Borsje, B.W. and Roelvink, D.J.A. (2018). Do salt marshes survive sea level rise? Modelling wave action, morphodynamics and vegetation dynamics. *Environ. Modell. Softw.*, 109, 152-166. https://doi.org/10.1016/j.envsoft.2018.08.004

Brückner, M.Z.M., Schwarz, C., Dijk, W.M., Oorschot, M., Douma, H. and Kleinhans, M.G. (2019). Salt marsh establishment and eco-engineering effects in dynamic estuaries determined by species growth and mortality. *J. Geophys. Res.: Earth Surf*. 124(12), 2962-2986. https://doi.org/10.1029/2019jf005092

Cahoon, D.R., White, D.A. and Lynch, J.C. (2011). Sediment infilling and wetland formation dynamics in an active crevasse splay of the Mississippi River delta. *Geomorphology*, 131(3-4), 57-68. https://doi.org/10.1016/j.geomorph.2010.12.002

Caldwell, R.L. and Edmonds, D.A. (2014). The effects of sediment properties on deltaic processes and morphologies: A numerical modeling study. *J. Geophys. Res.: Earth Surf.*, 119(5), 961-982. https://doi.org/10.1002/2013jf002965

Cao, H., Zhu, Z., Balke, T., Zhang, L. and Bouma, T.J. (2018). Effects of sediment disturbance regimes on Spartina seedling establishment: Implications for salt marsh creation and restoration. *Limnol. Oceanogr.*, 63(2), 647-659. https://doi.org/10.1002/lno.10657

Caponi, F., Koch, A., Bertoldi, W., Vetsch, D.F. and Siviglia, A. (2019). When Does Vegetation Establish on Gravel Bars? Observations and Modeling in the Alpine Rhine River. *Front. Environ. Sci.*, 7, 124. https://doi.org/10.3389/fenvs.2019.00124

Carle, M.V. and Sasser, C.E. (2016). Productivity and Resilience: Long-Term Trends and Storm-Driven Fluctuations in the Plant Community of the Accreting Wax Lake Delta. *Estuar. Coast.*, 39, 406-422. https://doi.org/10.1007/s12237-015-0005-9

Carle, M.V., Sasser, C.E. and Roberts, H.H. (2015). Accretion and Vegetation Community Change in the Wax Lake Delta Following the Historic 2011 Mississippi River Flood. *J. Coast. Res.*, 31(3), 569-587. https://doi.org/10.2112/jcoastres-d-13-00109.1

Cui, B., Yang, Q., Yang, Z. and Zhang, K. (2009). Evaluating the ecological performance of wetland restoration in the Yellow River Delta, China. *Ecol. Eng.*, 35(7), 1090-1103. https://doi.org/10.1016/j.

ecoleng.2009.03.022

de Groot, R., Brander, L., van der Ploeg, S., Costanza, R., Bernard, F., Braat, L., Christie, M., Crossman, N., Ghermandi, A., Hein, L., Hussain, S., Kumar, P., McVittie, A., Portela, R., Rodriguez, L.C., ten Brink, P. and van Beukeringh, P. (2012). Global estimates of the value of ecosystems and their services in monetary units. *Ecosyst. Serv.*, 1(1), 50-61. https://doi.org/10.1016/j.ecoser.2012.07.005

Deng, Z.F., Deng, Z.W., An, S.Q., Wang, Z.S., Liu, Y.H., Ouyang, Yan., Zhou, C.F., Zhi, Y.B. and Li, H.L. (2009). Habitat choice and seed-seedling conflict of Spartina alterniflora on the coast of China. *Hydrobiologia*, 630, 287-297. https://doi.org/10.1007/s10750-009-9822-9

Edmonds, D.A. and Slingerland, R.L. (2010). Significant effect of sediment cohesion on delta morphology. *Nat. Geosci.*, 3, 105-109. https://doi.org/10.1038/ngeo730

Elsey-Quirk, T., Graham, S.A., Mendelssohn, I.A., Snedden, G., Day, J.W., Twilley, R.R., Shaffer, G., Sharp, L.A., Pahl, J. and Lane, R.R. (2019). Mississippi river sediment diversions and coastal wetland sustainability: Synthesis of responses to freshwater, sediment, and nutrient inputs. *Estuar. Coast. Shelf Sci.*, 221, 170-183. https://doi.org/10.1016/j.ecss.2019.03.002

Ezcurra, E., Barrios, E., Ezcurra, P., Ezcurra, A., Vanderplank, S., Vidal, O., Villanueva-Almanza, L. and Aburto-Oropeza, O. (2019). A natural experiment reveals the impact of hydroelectric dams on the estuaries of tropical rivers. *Sci. Adv.*, 5(3), eaau9875. https://doi.org/10.1126/sciadv.aau9875

Fagherazzi, S., Edmonds, D.A., Nardin, W., Leonardi, N., Canestrelli, A., Falcini, F., Jerolmack, D.J., Mariotti, G., Rowland, J.C. and Slingerland, R.L. (2015). Dynamics of river mouth deposits. *Rev. Geophys.*, 53(3), 642-672. https://doi.org/10.1002/2014rg000451

Fagherazzi, S., Kirwan, M.L., Mudd, S.M., Guntenspergen, G.R., Temmerman, S., D'Alpaos, A., van de Koppel, J., Rybczyk, J.M., Reyes, E., Craft, C. and Clough, J. (2012). Numerical models of salt marsh evolution: Ecological, geomorphic, and climatic factors. *Rev. Geophys.*, 50(1), RG1002. https://doi.org/10.1029/2011rg000359

Ganju, N.K. (2019). Marshes Are the New Beaches: Integrating Sediment Transport into Restoration Planning. *Estuar. Coast.*, 42, 917-926. https://doi.org/10.1007/s12237-019-00531-3

Gao, W.L., Shao, D.D., Wang, Z.B., Nardin, W., Rajput, P., Yang, W., Sun, T. and Cui, B.S. (2019). Long-term cumulative effects of intra-annual variability of unsteady river discharge on the progradation of Delta Lobes: A Modeling Perspective. *J. Geophys. Res.: Earth Surf.*, 124(4), 960-973. https://doi.org/10.1029/2017JF004584

Gao, W.L., Shao, D.D., Wang, Z.B., Nardin, W., Yang, W., Sun, T. and Cui, B.S. (2018). Combined Effects of Unsteady River Discharges and Wave Conditions on River Mouth Bar Morphodynamics. *Geophys. Res. Lett.*, 45(23), 12903-12911. https://doi.org/10.1029/2018GL080447

Ge, Z.M., Cao, H.B., Cui, L.F., Zhao, B. and Zhang, L.Q. (2015a). Future vegetation patterns and primary production in the coastal wetlands of East China under sea level rise, sediment reduction, and saltwater intrusion. *J. Geophys. Res.: Biogeosci.*, 120(10), 1923-1940. https://doi.org/10.1002/2015JG003014

Ge, Z.M., Cao, H.B. and Zhang, L.Q. (2013). A process-based grid model for the simulation of range expansion of Spartina alterniflora on the coastal saltmarshes in the Yangtze Estuary. *Ecol. Eng.*, 58, 105-112. https://doi.org/10.1016/j.ecoleng.2013.06.024

Ge, Z.M., Zhang, L.Q. and Yuan, L. (2015b). Spatiotemporal Dynamics of Salt Marsh Vegetation regulated by Plant Invasion and Abiotic Processes in the Yangtze Estuary: Observations with a Modeling Approach. *Estuar. Coast.*, 38, 310-324. https://doi.org/10.1007/s12237-014-9804-7

Guo, X.B. (2013). Characteristics of recent tidal current and suspended sediment concentration distribution and sediment transport in the Yangtze Estuary. M.S. Dissertation, State Key Laboratory Of Estuarine and Coastal Research, East China Normal University, Shanghai, China.

He, Q., Cui, B.S., Cai, Y.Z., Deng, J.F., Sun, T. and Yang, Z.F. (2009). What confines an annual plant to two separate zones along coastal topographic gradients? *Hydrobiologia*, 630, 327-340. https://doi.org/10.1007/s10750-009-9825-6

Hiatt, M., Snedden, G., Day, J.W., Rohli, R.V., Nyman, J.A., Lane, R. and Sharp, L.A. (2019). Drivers and impacts of water level fluctuations in the Mississippi River delta: Implications for delta restoration. *Estuar. Coast. Shelf Sci.*, 224, 117-137. https://doi.org/10.1016/j.ecss.2019.04.020

Hu, M., Ge, Z., Li, Y., Li, S., Tan, L., Xie, L., Hu, Z., Zhang, T. and Li, X. (2019). Do short-term increases in river and sediment discharge determine the dynamics of coastal mudflat and vege- tation in the Yangtze Estuary? *Estuar. Coast. Shelf Sci.*, 220, 176-184. https://doi.org/10.1016/j.ecss.2019.03.004

Hu, Z., van Belzen, J., van der Wal, D., Balke, T., Wang, Z.B., Stive, M. and Bouma, T.J. (2015). Windows of opportunity for salt marsh vegetation establishment on bare tidal flats: The importance of temporal and spatial variability in hydrodynamic forcing. *J. Geophys. Res.: Biogeosci.*, 120(7), 1450-1469. https://doi.org/10.1002/2014JG002870

Huang, H.M., Zhang, L.Q., Guan, Y.J. and Wang, D.H. (2008). A cellular automata model for population expansion of Spartina alterniflora at Jiuduansha Shoals, Shanghai, China. *Estuar. Coast. Shelf Sci.*, 77, 47-55. https://doi.org/10.1016/j.ecss.2007.09.003

Kearney, M.S., Riter, J.C.A. and Turner, R.E. (2011). Freshwater river diversions for marsh restoration in Louisiana: Twenty-six years of changing vegetative cover and marsh area. *Geophys. Res. Lett.*, 38, L16405. https://doi.org/10.1029/2011gl047847

Ladd, C.J.T., Duggan-Edwards, M.F., Bouma, T.J., Pagès, J.F. and Skov, M.W. (2019). Sediment Supply Explains Long – Term and Large – Scale Patterns in Salt Marsh Lateral Expansion and Erosion. *Geophys. Res. Lett.*, 46, 11178-11187. https://doi.org/10.1029/2019gl083315

Latrubesse, E.M. (2008). Patterns of anabranching channels: The ultimate end-member adjustment of mega rivers. *Geomorphology*, 101, 130-145. https://doi.org/10.1016/j.geomorph.2008.05.035

Leonardi, N., Canestrelli, A., Sun, T. and Fagherazzi, S. (2013). Effect of tides on mouth bar morphology and hydrodynamics. *J. Geophys. Res.: Oceans*, 118, 4169-4183. https://doi.org/10.1002/ jgrc.20302

Lera, S., Nardin, W., Sanford, L., Palinkas, C. and Guercio, R. (2019). The impact of submersed aquatic vegetation on the development of river mouth bars. *Earth Surf. Process. Landf.*, 44, 1494-1506. https://doi.org/10.1002/esp.4585

Lesser, G.R., Roelvink, J.A., van Kester, J.A.T.M. and Stelling, G.S. (2004). Development and validation of a three-dimensional morphological model. *Coast. Eng.*, 51, 883-915. https://doi.org/10.1016/j.coastaleng.2004.07.014

Li, R., Yu, Q., Wang, Y., Wang, Z.B., Gao, S. and Flemming, B. (2018). The relationship between inundation duration and Spartina alterniflora growth along the Jiangsu coast, China. *Estuar. Coast. Shelf Sci.*, 213, 305-313. https://doi.org/10.1016/j.ecss.2018.08.027

Liu, H.Y., Lin, Z.S., Qi, X.Z., Zhang, M.Y. and Yang, H. (2014). The relative importance of sexual and asexual reproduction in the spread of Spartina alterniflora using a spatially explicit individual-based model. *Ecol. Res.*, 29, 905-915. https://doi.org/10.1007/s11284-014-1181-y

Liu, Z., Fagherazzi, S. and Cui, B. (2021). Success of coastal wetlands restoration is driven by sediment availability. *Commun. Earth Environ.*, 2, 44. https://doi.org/10.1038/s43247-021-00117-7

Ma, H., Nittrouer, J.A., Naito, K., Fu, X., Zhang, Y., Moodie, A.J., Wang, Y., Wu, B. and Parker, G. (2017). The exceptional sediment load of fine-grained dispersal systems: Example of the Yellow River, China. *Sci. Adv.*, 3, e1603114. https://doi.org/10.1126/sciadv.1603114

Nardin, W. and Edmonds, D.A. (2014). Optimum vegetation height and density for inorganic sedimentation in deltaic marshes. *Nat.*

Geosci., 7, 722-726. https://doi.org/10.1038/ngeo2233
Ning, Z., Chen, C., Xie, T., Wang, Q., Bai, J., Shao, D., Man, Y. and Cui, B. (2020). Windows of opportunity for smooth cordgrass landward invasion to tidal channel margins: The importance of hydrodynamic disturbance to seedling establishment. *J. Environ. Manage.*, 266, 110559. https://doi.org/10.1016/j.jenvman.2020.110559
Ning, Z., Chen, C., Zhu, Z., Xie, T., Wang, Q., Cui, B. and Bouma, T. J. (2021). Tidal channel-mediated gradients facilitate Spartina alterniflora invasion in coastal ecosystems: implications for invasive species management. *Mar. Ecol.: Prog. Ser.*, 659, 59-73. https://doi.org/10.3354/meps13560
Odink, S.J. (2019). Long-term marsh growth and retreat in an online coupled hydrodynamic, morphodynamic and ecological model. M.S. Dissertaion, Water Engineering and Management Faculty of Engineering Technology, University of Twente, Twente, Netherland.
Olliver, E.A., Edmonds, D.A. and Shaw, J.B. (2020). Influence of Floods, Tides, and Vegetation on Sediment Retention in Wax Lake Delta, Louisiana, USA. *J. Geophys. Res.: Earth Surf.*, 125(1), e2019-JF005316. https://doi.org/10.1029/2019jf005316
Pasquale, N., Perona, P., Francis, R. and Burlando, P. (2014). Above-ground and below-ground Salixdynamics in response to river processes. *Hydrol. Process.*, 28(20), 5189-5203. https://doi.org/10.1002/hyp.9993
Peyronnin, N., Caffey, R., Cowan, J., Justic, D., Kolker, A., Laska, S., McCorquodale, A., Melancon, E., Nyman, J., Twilley, R., Visser, J., White, J. and Wilkins, J. (2017). Optimizing Sediment Diversion Operations: Working Group Recommendations for Integrating Complex Ecological and Social Landscape Interactions. *Water*, 9(6), 368. https://doi.org/10.3390/w9060368
Ruth, M. and Brian, D.R. (2007). Application of the Indicators of Hydrologic Alteration Software in Environmental Flow Setting. *J. Am. Water Resour. Assoc.*, 43(6), 1400-1413. https://doi.org/10.1111/j.1752-1688.2007.00099.x
Schwarz, C., Gourgue, O., van Belzen, J., Zhu, Z., Bouma, T.J., van de Koppel, J., Ruessink, G., Claude, N. and Temmerman, S. (2018). Self-organization of a biogeomorphic landscape controlled by plant life-history traits. *Nat. Geosci.*, 11, 672-677. https://doi.org/10.1038/s41561-018-0180-y
Shaw, J.B., Mohrig, D. and Whitman, S.K. (2013). The morphology and evolution of channels on the Wax Lake Delta, Louisiana, USA. *J. Geophys. Res.: Earth Surf.*, 118(3), 1562-1584. https://doi.org/10.1002/jgrf.20123
Smis, A., Van Damme, S., Struyf, E., Clymans, W., Van Wesemael, B., Frot, E., Vandevenne, F., Van Hoestenberghe, T., Govers, G. and Meire, P. (2010). A trade-off between dissolved and amorphous silica transport during peak flow events (Scheldt river basin, Belgium): impacts of precipitation intensity on terrestrial Si dynamics in strongly cultivated catchments. *Biogeochemistry*, 106, 475-487. https://doi.org/10.1007/s10533-010-9527-1
Suchrow, S. and Jensen, K. (2010). Plant Species Responses to an Elevational Gradient in German North Sea Salt Marshes. *Wetlands*, 30, 735-746. https://doi.org/10.1007/s13157-010-0073-3
Sun, Z., Mou, X., Lin, G., Wang, L., Song, H. and Jiang, H. (2010). Effects of sediment burial disturbance on seedling survival and growth of Suaeda salsa in the tidal wetland of the Yellow River estuary. *Plant Soil*, 337, 457-468. https://doi.org/10.1007/s11104-010-0542-8
Syvitski, J.P.M. and Saito, Y. (2007). Morphodynamics of deltas under the influence of humans. *Glob. Planet. Change*, 57(3-4), 261-282. https://doi.org/10.1016/j.gloplacha.2006.12.001
Szczypta, C., Decharme, B., Carrer, D., Calvet, J.C., Lafont, S., Somot, S., Faroux, S. and Martin, E. (2012). Impact of precipitation and land biophysical variables on the simulated discharge of European and Mediterranean rivers. *Hydrol. Earth Syst. Sci.*, 16, 3351- 3370. https://doi.org/10.5194/hess-16-3351-2012
Takahashi, D., Sim, S.W. and Park, E.J. (2019). Colonial population dynamics of Spartina alterniflora. *Ecol. Model.*, 395, 45-50. https://doi.org/10.1016/j.ecolmodel.2019.01.013
Taylor, C.M., Davis, H.G., Civille, J.C., Grevstad, F.S. and Hastings, A. (2004). Consequences of an Allee effect in the invasion of a pacific estuary by *Spartina alterniflora*. *Ecology*, 85(12), 3254-3266. https://doi.org/10.1890/03-0640
Taylor, C.M. and Hastings, A. (2004). Finding optimal control strategies for invasive species: a density-structured model for Spartina alterniflora. *J. Appl. Ecol.*, 41(6), 1049-1057. https://doi.org/10.1111/j.0021-8901.2004.00979.x
Twilley, R.R., Day, J.W., Bevington, A.E., Castañeda-Moya, E., Christensen, A., Holm, G., Heffner, L.R., Lane, R., McCall, A., Aarons, A., Li, S., Freeman, A. and Rovai, A.S. (2019). Ecogeomorphology of coastal deltaic floodplains and estuaries in an active delta: Insights from the Atchafalaya Coastal Basin. *Estuar. Coast. Shelf Sci.*, 227, 106341. https://doi.org/10.1016/j.ecss.2019.106341
Vilas, M.P., Adams, M.P., Oldham, C.E., Marti, C.L. and Hipsey, M.R. (2017). Fragment dispersal and plant-induced dieback explain irregular ring-shaped pattern formation in a clonal submergeed macrophyte. *Ecol. Model.*, 363, 111-121. https://doi.org/10.1016/j.ecolmodel.2017.09.001
Wang, H.J., Wu, X., Bi, N.S., Li, S., Yuan, P., Wang, A.M., Syvitski, J.P.M., Saito, Y., Yang, Z.S., Liu, S.M. and Nittrouer, J. (2017). Impacts of the dam-orientated water-sediment regulation scheme on the lower reaches and delta of the Yellow River (Huanghe): A review. *Glob. Planet. Change*, 157, 93-113. https://doi.org/10.1016/j.gloplacha.2017.08.005
Wang, Z.B., Vandenbruwaene, W., Taal, M. and Winterwerp, H. (2019). Amplification and deformation of tidal wave in the Upper Scheldt Estuary. *Ocean Dyn.*, 69, 829-839. https://doi.org/10.1007/s10236-019-01281-3
Wintenberger, C.L., Rodrigues, S., Greulich, S., Bréhéret, J.G., Jugé, P., Tal, M., Dubois, A. and Villar, M. (2019). Control of Non-migrating Bar Morphodynamics on Survival of Populus nigra Seedlings during Floods. *Wetlands*, 39, 275-290. https://doi.org/10.1007/s13157-018-1121-7
Xiao, D.R., Zhang, L.Q. and Zhu, Z.C. (2009). A study on seed characteristics and seed bank of Spartina alterniflora at saltmarshes in the Yangtze Estuary, China. *Estuar. Coast. Shelf Sci.*, 83(1), 105-110. https://doi.org/10.1016/j.ecss.2009.03.024
Xue, L., Li, X., Yan, Z., Zhang, Q., Ding, W., Huang, X., Tian, B., Ge, Z. and Yin, Q. (2017). Native and non-native halophytes resiliency against sea-level rise and saltwater intrusion. *Hydrobiologia*, 806, 47-65. https://doi.org/10.1007/s10750-017-3333-x
Yang, W., Wang, Q., Pan, X. and Li, B. (2014). Estimation of the Probability of Long-Distance Dispersal: Stratified Diffusion of *Spartina alterniflora* in the Yangtze River Estuary. *American J. of Plant Sci.*, 5(24), 3642-3651. https://doi.org/10.4236/ajps.2014.524380
Zhang, H., Chen, X. and Luo, Y. (2016). An overview of ecohydrology of the Yellow River delta wetland. *Ecohydrol. Hydrobiol.*, 16(1), 39-44. https://doi.org/10.1016/j.ecohyd.2015.10.001
Zheng, S., Shao, D. and Sun, T. (2018). Productivity of invasive saltmarsh plant Spartina alterniflora along the coast of China: A meta-analysis. *Ecol. Eng.*, 117, 104-110. https://doi.org/10.1016/j.ecoleng.2018.03.015
Zhou, Z., Olabarrieta, M., Stefanon, L., D'Alpaos, A., Carniello, L. and Coco, G. (2014). A comparative study of physical and numerical modeling of tidal network ontogeny. *J. Geophys. Res.: Earth Surf.*, 119(4), 892-912. https://doi.org/10.1002/2014jf003092